J. Fluid Mech. (2007), *vol.* 576, *pp.* 325–348.
doi:10.1017/S0022112006004447 Printed in the United Kingdom

Centre modes in inviscid swirling flows and their application to the stability of the Batchelor vortex

C. J. HEATON

Department of Applied Mathematics and Theoretical Physics, University of Cambridge, Wilberforce Road, Cambridge CB3 0WA, UK

(Received 7 April 2006 and in revised form 10 October 2006)

We identify a family of centre-mode disturbances to inviscid swirling flows such as jets, wakes and other vortices. The centre modes form an infinite family of modes, increasingly concentrated near to the symmetry axis of the mean flow, and whose frequencies accumulate to a single point in the complex plane. This asymptotic accumulation allows analytical progress to be made, including a theoretical stability boundary, in $O(1)$ parameter regimes. The modes are located close to the continuous spectrum of the linearized Euler equations, and the theory is closely related to that of the continuous spectrum. We illustrate our analysis with the inviscid Batchelor vortex, defined by swirl parameter q. We show that the inviscid instabilities found in previous numerical studies are in fact the first members of an infinite set of centre modes of the type we describe. We investigate the inviscid neutral curve, and find good agreement of the neutral curve predicted by the analysis with the results of numerical computations. We find that the unstable region is larger than previously reported. In particular, the value of q above which the inviscid vortex stabilizes is significantly larger than previously reported and in agreement with a long-standing theoretical prediction.

1. Introduction

The stability of vortices is a topic with wide ranging applications and has accordingly received much attention from researchers, both experimental and theoretical. Swirling pipe flow, the trailing line vortex from an aeroplane wing and many other instances of vortex breakdown provide applications for the theory we present. We will concentrate here on Batchelor's (1964) model of the trailing line vortex as our prototype flow. In the last few years numerical observations have uncovered many complicated aspects of this problem. The aim of this paper is to describe the mathematical structure of the inviscid instabilities, one aspect of the larger problem.

There is an enormous literature available on vortex stability, dating back to Rayleigh (1916) and the famous stability criterion for axisymmetric rotating fluid. More recently the attention of theoreticians has been concentrated on two particular flows. Rotating pipe flow has been investigated by many, a representative sample of the published work being the papers by Maslowe (1974), Maslowe & Stewartson (1974), Wang & Rusak (1996) and Cotrell & Pearlstein (2004). Analytical progress has been largely confined to the regime of asymptotically large azimuthal wavenumber; see Maslowe & Stewartson (1974) and related papers.

Even more attention has been focused on the Batchelor vortex (also known as the trailing line or q vortex), and it is on this example that we focus our attention in the

present paper. Numerical studies have been carried out by Lessen, Singh & Paillet (1974), Duck & Foster (1980) and Mayer & Powell (1992) in the case of inviscid flow. Finite-Reynolds-number calculations have been performed by Lessen & Paillet (1974), Khorrami (1991), Mayer & Powell (1992) and Fabre & Jacquin (2004), the latter being able to reach values of $Re \simeq 10^6$ (Re based on the vortex core radius and core axial velocity). Instabilities of a purely viscous nature were first found by Khorrami (1991), who observed growth rates which decay as Re^{-1} in the limit $Re \to \infty$. More recently, Fabre & Jacquin (2004) have observed viscous modes with growth rates decaying as $Re^{-1/3}$, and a large-Re asymptotic description of these is given by Le Dizès & Fabre (2006) (N B the first appearance of these modes appears to be in figure 24 of Olendraru & Sellier 2002). For all known viscous modes, a maximum growth rate occurs, usually $O(10^{-2})$ or smaller, at a finite value of Re. In contrast, the inviscid modes have growth rates which increase to a finite limit as $Re \to \infty$, the largest inviscid growth rate being 0.46 (see Mayer & Powell 1992). The inviscid growth rates increase with m (m being the azimuthal wavenumber; see Leibovich & Stewartson 1983), but so does the action of viscous damping. These two effects were balanced by Denier & Stott (2005), who found the largest growth rates at finite Re by taking the scaling $m \sim Re^{1/2}$.

Few general analytical results are available for the stability of swirling flows. Perhaps the most significant result is the sufficient criterion for instability derived by Leibovich & Stewartson (1983). This result was achieved via large-$|m|$ asymptotics for the inviscid case, and a number of follow-up papers used similar analyses to give more details of the large-$|m|$ stability boundaries. For the Batchelor vortex Leibovich & Stewartson's criterion implies instability for $q < \sqrt{2}$. Numerical studies have found that the flow is inviscidly stable for mean swirl numbers greater than $q \simeq 1.5$, a figure first found by Lessen *et al.* (1974) and later by Mayer & Powell (1992) and others. However, the other theoretical result of particular relevance is that of Stewartson & Brown (1985), who performed a remarkable near-neutral asymptotic analysis at finite $|m|$. They found that, asymptotically close to the neutral point, the inviscid instabilities were of a centre-mode type, and that the vortex becomes stabilized at $q = 2.31$. Previous numerical calculations of the inviscid problem, however, have not found unstable modes at any swirl numbers greater than $q \simeq 1.5$. Thus a discrepancy has existed between the prediction of Stewartson & Brown (1985) and the results of numerical calculations for some time. The value $q \simeq 1.5$ appears to have been most widely accepted: for example, Ash & Khorrami (1995), Loiseleux, Chomaz & Huerre (1998), Delbende, Chomaz & Huerre (1998), Fabre & Jacquin (2004) and Le Dizès & Fabre (2006) all quote the $q \simeq 1.5$ result. The location of this 'upper neutral point', the swirl level at which the inviscid instabilities are neutralized, is important to the wider problem because vortex breakdown is often observed at $q \gtrsim 2$ (Leibovich 1978). Inviscid instabilities, which for smaller q are the strongest of all instabilities, have not been found at such large values of q and so it is assumed that other effects must be responsible: for example the viscous modes of Fabre & Jacquin (2004) exist at all swirl levels if Re is sufficiently large, and so may provide such a mechanism. Clarification of the location of the inviscid neutral curve and its upper neutral point is important for this reason, and is one of the problems we consider.

In the context of the above review of the relevant literature, the new results of the present paper can be summarized. We restrict our attention to purely inviscid flow, and show that there exist centre modes, which can be stable or unstable. The modes have their asymptotic centre-mode form for generic $O(1)$ parameters (rather than in a large-$|m|$, near-neutral, or other parameter limit) and they form an infinite

set of eigenvalue frequencies (in a temporal analysis, correspondingly wavenumbers in a spatial analysis). Our analysis also yields a new theoretical prediction for the location of the stability boundary. We consider the Batchelor vortex as a case study, for which it is demonstrated that the inviscid instabilities, as found by several previous numerical studies, are in fact centre modes of the type we describe. Using numerical methods which are suited to the asymptotic structure of the centre modes, and which produce no spurious results, we are able to find many more of the higher-order modes. We also investigate the neutral curve for the inviscid modes, and find good agreement between the theoretical predictions and numerical computations. Further, both our computational and our theoretical neutral curves agree with the result of Stewartson & Brown (1985) that the inviscid Batchelor vortex is stabilized for $q > 2.31$. At this point, and also around the rest of the neutral curve, our asymptotics and numerics disagree with the previously reported numerical results. We believe that the previous numerical results are in error, as a result of the characteristic structure of the centre modes (which lie close to the continuous spectrum) and also the peculiar shape of the neutral curve (which has a very narrow tongue extending to larger q), two factors which make computations difficult. Our numerical method is chosen to resolve the centre-mode asymptotic structure as well as possible, whereas some other methods are not as suitable for this purpose, something we discuss in detail later. As a result, the previous numerical work has missed unstable modes for $q > 1.5$, and we will present for the first time numerically obtained inviscid modes in the range $1.5 < q < 2.31$.

Recently Heaton & Peake (2006) (herein referred to as I) reported various stability results for inviscid compressible swirling flow in an annular pipe. The present paper extends the theory of I to vortices with no centre body, and so we briefly review the findings of I here. Starting from the standard Briggs–Bers method, the continuous spectrum of the linearized Euler equations was identified and its contribution to a generic unsteady field was described and calculated. Intimately related to the continuous spectrum, hydrodynamic *nearly convected* modes were described which comprise an infinite set or sets of modes which accumulate in the complex frequency-plane (in a temporal analysis, or the wavenumber-plane in a spatial analysis) towards a point in the continuous spectrum. The infinite accumulation of frequency (or wavenumber) eigenvalues allows analytical progress to be made and the asymptotic accumulation of wall modes (stable) and ring modes (stable or unstable, localized on a radius within the annular duct) was described. It was found in I that the continuous spectrum can cause a new algebraic instability, significantly stronger than the linear growth of the 'lift-up' effect in two-dimensional shear flow (see Landahl 1980). This effect is also present in the flows we consider here, such as the Batchelor vortex, but for now we concentrate our attention on the exponential (discrete) instability modes. The results of I reviewed here were purely hydrodynamic in nature, unaffected by compressibility. In the present paper, as we extend the relevant theory of I to vortices with no centre body, we restrict attention to incompressible flow for simplicity. The analysis we present for the centre modes is an extension of the treatment of ring modes given in I. It is a broadly similar asymptotic problem, but with several important differences in the calculation. In particular, these differences mean that for the centre modes a theoretical stability boundary can be derived, something not available for the ring modes in I.

The remainder of this paper is set out as follows. In § 2 the governing equations and their relevant singularity structure are discussed. In § 3 we perform the asymptotic calculation which defines unstable centre modes and derive a related stability criterion. In § 4 we outline the analogous calculation for stable centre modes. In § 5 we turn to apply our ideas to the Batchelor vortex: we show that the analysis of § 3 applies, and

we also perform direct numerical calculations to investigate the instabilities. In § 5.4 we turn to investigate the inviscid neutral curve, concentrating especially on $m = -1$. Some final conclusions are drawn in § 6.

2. The governing equations

We consider unsteady perturbations to incompressible inviscid fluid with a cylindrically symmetric mean flow which is of swirling jet or wake type. The flow may be confined in a cylindrical pipe or unconfined as the case may be. We use cylindrical polar coordinates (x, r, θ) and lengths, densities and velocities are non-dimensionalized by representative values of the mean flow, e.g. the pipe radius or the vortex core radius. The incompressible flow has total velocity

$$\boldsymbol{U}_{tot}(x, r, \theta, t) = \boldsymbol{U}_0(r) + \boldsymbol{u}(x, r, \theta, t), \tag{2.1}$$

being the steady mean flow plus a small unsteady perturbation. The mean flow we consider takes the form

$$\boldsymbol{U}_0 = U(r)\boldsymbol{e}_x + W(r)\boldsymbol{e}_\theta. \tag{2.2}$$

We impose some restrictions on the inviscid mean flows to be considered, namely

$$W(0) = U'(0) = 0, \tag{2.3}$$

$$W''(0) = W^{(\mathrm{iv})}(0) = U'''(0) = 0, \tag{2.4}$$

which, we argue, are natural conditions to place on real-life flows. Condition (2.3) simply ensures that the velocity and pressure are non-singular on the coordinate axis $r = 0$, while (2.4) is satisfied by profiles which realistically model high-Reynolds-number viscous flows. Firstly, rotating Poiseuille flow, which is the exact solution of the Navier–Stokes having the form (2.2), automatically satisfies (2.4). Secondly, it is also seen that (2.4) holds for all the most commonly used vortex models, including the Rankine, Burgers, Lamb–Oseen and Batchelor vortices. In all cases (2.4) results from the nature of the approximation or similarity solution applied to the Navier–Stokes equations, and so would seem to be an acceptable condition on profiles modelling real high-speed flows. Our comments above notwithstanding, not all inviscid vortex models satisfy (2.4), for example the *ad hoc* profiles of Carton & McWilliams (1989), so we will mention briefly the formal behaviour in such cases also.

The Euler equations linearized about the mean flow (2.2) can be reduced to a single ODE for the radial component v of the perturbation velocity, as was done by Howard & Gupta (1962). Suppose all perturbations are Fourier-decomposed so that

$$\boldsymbol{u}(x, r, \theta, t) = \boldsymbol{u}(r)\mathrm{e}^{-\mathrm{i}\omega t + \mathrm{i}kx + \mathrm{i}m\theta}, \tag{2.5}$$

where m is the integer azimuthal wavenumber, k the axial wavenumber and ω the frequency. We seek solutions of the governing equations which are *causal*, or equivalently which are *bona fide* limits of viscous solutions in the limit of vanishing viscosity (a point discussed by Olendraru *et al.* 1999). This is achieved by following the Briggs–Bers technique (Briggs 1964; Bers 1983) for deforming the relevant Fourier inversion contours. For simplicity we consider the temporal stability problem, so that k is given and fixed throughout the analysis. Equivalently one could consider the spatial problem by considering ω as given and fixed, and the results and methodology are almost exactly the same. The relevant theory from I was performed for a spatial problem, but here we work in the temporal framework to enable direct comparison with previous published results when we come to apply our work to the case of the

Batchelor vortex. In general it is the physical context of a problem which determines whether a temporal or spatial framework is more relevant.

To proceed we define

$$\Lambda(k, \omega, r) = Uk - \omega + mW/r, \tag{2.6}$$

corresponding to the Lagrangian derivative operator D_0/Dt. We also let

$$\omega_c(r) = U(r)k + mW(r)/r, \tag{2.7}$$

which, since $\Lambda(k, \omega_c(r), r) \equiv 0$, is the frequency corresponding to pure convection of the unsteady perturbation by the mean flow at radius r. It will also be convenient to define the (typically complex and multivalued) inverse $r_c(k, \omega)$, such that

$$\Lambda(k, \omega, r_c(k, \omega)) \equiv 0. \tag{2.8}$$

Howard & Gupta's equation, the mode-shape equation, is then

$$\left(\frac{r}{(m^2 + k^2r^2)}(vr)'\right)' - \left\{1 + \frac{r}{\Lambda}\left(\frac{r^2\Lambda' + 2mW}{r(m^2 + k^2r^2)}\right)' - \frac{2kW(k(Wr)' - mU')}{(m^2 + k^2r^2)\Lambda^2}\right\} v = 0, \tag{2.9}$$

where prime denotes differentiation with respect to r. The boundary conditions to be applied to (2.9) are $v = 0$ at the pipe wall if present, or $v \to 0$ as $r \to \infty$ if the flow is unconfined. Since we wish to consider flows with no centre body, at $r = 0$ the regularity conditions derived by Batchelor & Gill (1962) must be applied; here they reduce (using (2.3)–(2.4)) to

$$\left.\begin{aligned} v(0) &= 0, \qquad |m| \neq 1, \\ v'(0) &= 0, \qquad |m| = 1. \end{aligned}\right\} \tag{2.10}$$

In fact, the details of the boundary condition to be applied at $r = 0$ will not prove to be very important; rather the fact that a real boundary condition of some sort must be applied will be enough to generate the centre-mode behaviour we describe.

2.1. *The singularity structure of the governing equation*

The mode-shape equation (2.9) is similar to the mode-shape equation (2.21) of I, the two differences being that here we assume the fluid to be incompressible and we take a different choice of dependent variable. Viewed as an ODE in r with k, ω & m fixed, (2.9) has singularities at $r = 0$ and at the *critical radius* $r = r_c(k, \omega)$ (i.e. when the coefficient of the highest derivative v'' is zero and when $\Lambda = 0$, respectively). The singularities are usually regular singular points (RSPs) of (2.9), and in this case an elementary Frobenius expansion, $v = \xi^\sigma \sum_0^\infty a_n \xi^n$ where $\xi = r - r^*$ and r^* is the singular radius, is possible. We find that

$$\sigma_0 = -1 \pm m, \tag{2.11}$$

$$\sigma_c = (1 \pm \sqrt{1 - 4A(r_c)})/2, \tag{2.12}$$

for the exponents at $r^* = 0$ and $r^* = r_c(k, \omega)$ respectively, where

$$A(r) \equiv \frac{2Wk\,(k(Wr)' - mU')}{r^2\omega_c'^2}, \tag{2.13}$$

and primes, as elsewhere, mean differentiation with respect to r. In the analysis to follow k will be fixed, so the notation of (2.13), in which $A(r)$ is written as a

function of r alone, will prove convenient. $A(r)$ is the same function that appeared in I and controls many related features of the spectrum, including the stability of the continuous spectrum and the presence and nature of ring and wall modes. We note that (2.12), which will prove to be a key ingredient in our analysis, is the same exponent as would be obtained if the flow were compressible (cf. (2.28) of I).

In solving any given temporal problem, after fixing k, we must invert the temporal Fourier transform along the relevant contour defined by the Briggs–Bers procedure: the correct Briggs–Bers inversion contour in the complex ω-plane passes *above* all singularities and modes. In particular this includes the continuous spectrum, given by

$$C_\omega = \{\omega_c(r)\}, \tag{2.14}$$

the set of frequencies for which a singular point r_c exists in the flow geometry. Because the solution to (2.9) cannot be holomorphic in ω for $\omega \in C_\omega$, C_ω defines a branch cut of the complex ω-plane and every frequency it contains contributes to the Fourier inversion. For some such frequencies the singularities of (2.9) cease to be regular, namely when $\omega = \omega_c(r^*)$ and additionally

$$\omega_c'(r^*) = 0, \tag{2.15}$$

in which case two RSPs merge and form a non-regular, or essential, singularity. In such cases the denominator of (2.13) vanishes. An essential singularity for which $r^* \neq 0$ corresponds to the ring modes and was treated in I.

Here we observe that (2.3)–(2.4) imply that $\omega_c'(0) = 0$, and hence for such flows there is *always* a frequency, $\omega = \omega_c(0)$, for which an essential singularity is present at $r = 0$. Let us define the real constant

$$\alpha_0 = \left. \frac{2kW'(2kW' - mU'')}{(kU'' + mW'''/3)^2} \right|_{r=0}, \tag{2.16}$$

for which it follows that

$$A(r) \sim \alpha_0 / r^2 \quad \text{as} \quad r \to 0. \tag{2.17}$$

The possibility for unstable centre modes will hinge on the sign of α_0, which we note has the same sign as the 'modified Rayleigh quantity' near the origin,

$$W((Wr)' - mU'/k). \tag{2.18}$$

Before beginning the calculation we briefly mention what happens if (2.3)–(2.4) do not hold (for example, they do not hold for the *ad hoc* vortex profiles of Carton & McWilliams 1989). In such cases $\omega_c'(0) \neq 0$, and as a result the boundary conditions at $r = 0$ do not give rise to the behaviour we will describe. Instead $r = 0$ simply acts like a pipe wall or any other boundary, and 'wall modes' of the type described in I, which are always stable, may be present. As mentioned above, (2.3)–(2.4) do hold for all commonly used vortex models and we believe they constitute a reasonable restriction to impose.

3. The case of $\alpha_0 < 0$ and unstable centre modes

We assume wavenumbers k, m are given real constants with $m \in \mathbb{Z}$, and seek the eigenvalue frequencies such that (2.9) is satisfied along with appropriate boundary conditions at $r = 0, \infty$ (or at an outer pipe wall, if applicable). In this section we assume

$$\alpha_0 \equiv -\nu^2 < 0, \tag{3.1}$$

Inner region:	$\bar{R} \equiv r/\lvert\epsilon\rvert = O(1)$
Intermediate region:	$R \equiv r/\lvert\epsilon\rvert^{1/2} = O(1)$
Outer region:	$r = O(1)$

TABLE 1. The three asymptotic regions in the unstable centre mode calculation, § 3.

and we look for complex frequencies given by

$$\omega = \omega_c(0) + \epsilon \equiv \omega_c(0) + \xi + \mathrm{i}\eta, \quad \xi, \eta \in \mathbb{R}, \tag{3.2}$$

with $|\epsilon| \ll 1$. We shall see that there are three distinguished asymptotic regions, which for clarity are defined together in table 1. We now look at each region in turn and use asymptotic matching to construct the solution to (2.9).

3.1. *Inner region*

In the inner region

$$\Lambda = -\epsilon + O(\epsilon^2), \tag{3.3}$$

and hence to leading order (2.9) reduces to

$$\frac{\mathrm{d}}{\mathrm{d}\bar{R}}\bar{R}\frac{\mathrm{d}}{\mathrm{d}\bar{R}}\bar{R}v = \left\{m^2 + \frac{\nu^2\omega_c''^2|\epsilon|^2\bar{R}^2}{\epsilon^2}\right\}v, \tag{3.4}$$

where $\omega_c''^2$ is evaluated at $r = 0$. Solving (3.4) and applying the regularity conditions (2.10), the inner-region solution is given correct to $O(1)$ by

$$v = \frac{1}{\bar{R}}J_{|m|}(-\mathrm{i}\nu\omega_c''\bar{R}|\epsilon|/\epsilon). \tag{3.5}$$

3.2. *Intermediate region*

In the intermediate region to leading order we have

$$\Lambda = -\epsilon + \omega_c''|\epsilon|R^2/2 + O(\epsilon^2). \tag{3.6}$$

The leading-order governing equation is thus found to be of WKBJ type,

$$\frac{\mathrm{d}^2\Phi}{\mathrm{d}R^2} = \frac{|\epsilon|\nu^2\omega_c''^2\Phi}{(-\epsilon + \omega_c''|\epsilon|R^2/2)^2} + O(1), \tag{3.7}$$

where we define $\Phi \equiv R^{3/2}v$ in order to simplify the appearance of the equation. Equation (3.7) can be solved and we find the two linearly independent solutions in the intermediate region are, transforming back to v,

$$v = f_{\pm}(R,\epsilon) \equiv R^{-3/2}\sqrt{1 - \frac{\omega_c''|\epsilon|R^2}{2\epsilon}}\exp\left\{\pm\sqrt{1 + \frac{2\nu^2\omega_c''}{\epsilon}}\tanh^{-1}\left(R\sqrt{\frac{\omega_c''|\epsilon|}{2\epsilon}}\right)\right\}. \tag{3.8}$$

Asymptotically matching (3.5) with the solutions (3.8) gives the correct solution in the intermediate region as

$$v \propto f_+(R,\epsilon) + \mathrm{e}^{\mathrm{i}\pi|m| + \mathrm{i}\pi/2}f_-(R,\epsilon). \tag{3.9}$$

The overall constant of proportionality in (3.9) does not matter as the whole problem is linear: we only need the relative proportions in which the two solutions (3.8) are present.

3.3. *Outer region*

Finally we consider the outer region where $r = O(1)$. In this region the leading-order governing equation does not simplify sufficiently to allow a general solution to be written down; however, we can still make progress. To leading order

$$\Lambda = \omega_c(r) - \omega_c(0), \tag{3.10}$$

and hence $r = 0$ is a double zero of Λ (recall that $\omega_c'(0) = 0$ for the vortices we consider). The leading-order equation in the outer region is obtained by setting $\epsilon = 0$ in (2.9) and (3.2), but cannot in general be solved analytically; to obtain two linearly independent outer-region solutions in practice requires a numerical calculation. A consequence of (3.10) is that $r = 0$ is an essential singularity of the leading-order equation and so we can at least obtain the $r \to 0$ behaviour using standard methods (see p. 76 of Bender & Orszag 1978). We choose formally to define two independent solutions $g_\pm(r)$ of the leading-order problem by using the $r \to 0$ asymptotics so that, after a little algebra,

$$g_\pm(r) \sim r^{-1/2} \exp\left\{ \pm \frac{2v}{r} \mp \frac{3r}{16v} \right\} \quad \text{as} \quad r \to 0. \tag{3.11}$$

We now must match (3.9) with a combination of $g_\pm(r)$ using (3.11) in order to complete the calculation. It is easily seen that $f_\pm(R, \epsilon)$ and $g_\pm(r)$ do indeed functionally match; however, the essential singularity leads to a technical difficulty. We wish to track the coefficients of both $g_\pm(r)$, but if we perform our matching procedure with real values of r then $g_-(r)$ is exponentially smaller than $g_+(r)$ for small r, and the matching rule will not yield the coefficient of $g_-(r)$. To overcome this difficulty we formally perform the matching procedure along the imaginary axis in the complex r-plane, which ensures that $g_\pm(r)$ are both of the same magnitude as $r \to 0$. We shall revisit this technicality later in § 5.1.

The matching can now proceed in a straightforward manner: away from $r = 0$ a boundary condition is applied in the outer region, such as decay at infinity in an unbounded fluid or $v = 0$ at a pipe wall. This determines an $O(1)$ constant Q such that

$$v \propto g_+(r) + Q g_-(r) \ \text{ in the outer region}, \tag{3.12}$$

which is to be matched as $r \to 0$ with (3.9) as $R \to \infty$. On comparing the various coefficients we find

$$\mathrm{i}\pi \sqrt{\frac{2v^2\omega_c''}{\epsilon}} - \mathrm{i}\pi|m| - \frac{\mathrm{i}\pi}{2} + \log Q = 2\pi n \mathrm{i}, \tag{3.13}$$

for some $n \in \mathbb{Z}$, and this determines ϵ and hence the frequency ω. Since $|\epsilon| \ll 1$, the mode number is large, $n \gg 1$. Because the neglected terms in (3.7) are $O(1)$, which follows directly from (2.3)–(2.4), the neglected terms in the WKBJ solution (3.8) are seen to be $O(\epsilon^{1/2})$ and so do not contribute any $O(1)$ terms to (3.13). This implies that (3.13) is correct to $O(1)$, and hence we can deduce that

$$\epsilon = \frac{v^2\omega_c''}{2n^2} + \frac{v^2\omega_c''}{2n^3}\left(\frac{\log Q}{\mathrm{i}\pi} - |m| - \frac{1}{2} \right) + O(n^{-4}). \tag{3.14}$$

This final result (3.14) shows that an infinite number of centre-mode solutions exist, labelled by increasing mode number n, and that far down the asymptotic tail the frequency ω is real to leading order. If we restrict our attention to unstable modes ($Im(\epsilon) > 0$) then the picture in the complex r-plane is as in figure 1(*a*). The regular singular points where $\Lambda = 0$ for a frequency as given by (3.14) are seen to lie close

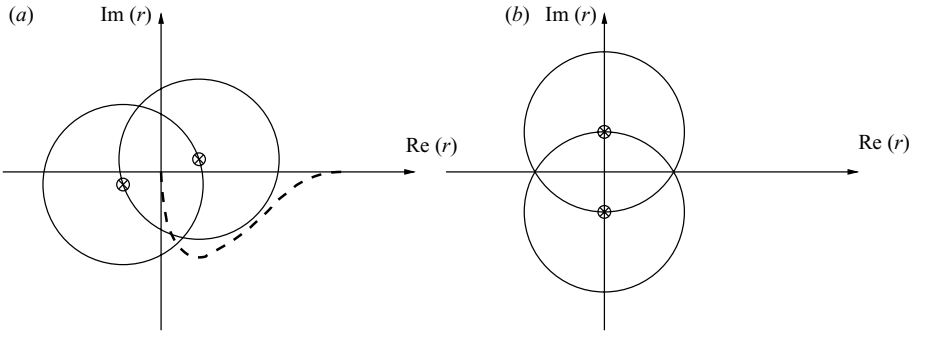

FIGURE 1. Schematic picture of the regular singular points (RSPs), shown by ⊗, together with corresponding circles of convergence. (*a*) $\alpha_0 < 0$, $Im(\epsilon) > 0$ (§3) shown in the case when $\omega_c''(0) > 0$. If $\omega_c''(0) < 0$ the picture is reflected in the real line. (*b*) When $\alpha_0 > 0$.

to the real line as shown. We see that analytic continuation off the real line so as to approach $r = 0$ along $\arg(r) = \text{sign}(-\omega_c''(0))\pi/2$ is possible, as depicted by the dashed line in figure 1(*a*), justifying the formal matching procedure described above.

The result of the calculation in this section is similar in many ways to the ring modes considered in I, with (3.14) implying that in the ω-plane the frequencies lie just above or below the continuous spectrum (see figure 2 below). Also, the Frobenius exponents (2.12) are found to be $O(|\epsilon|^{-1/2})$ large and real to leading order: this causes the solution v to be strongly peaked and highly oscillatory as r increases through real values past the singularity close to the real line in figure 1(*a*). Therefore the eigenmodes have rapid oscillations and are localized at

$$r \sim \sqrt{2\epsilon/\omega_c''} \sim \nu/n. \tag{3.15}$$

The oscillatory behaviour is not immediately visible in (3.8), but is hidden in the delicate behaviour of $\tanh^{-1}$ when its argument is close to unity. The radial velocity v therefore is concentrated and highly oscillatory in the intermediate region, and this justifies the term *centre mode*.

The present calculation differs from the analysis in I in several ways, most obviously the presence of a genuine third asymptotic region, the inner region, which deals with the complications of the Batchelor & Gill regularity conditions at the coordinate axis. Ultimately the most significant difference actually results from the relatively minor point that the error term in (3.7) is smaller than its equivalent in the ring-mode calculation of I. This in turn means that (3.14) is correct to second order and we can read off the growth rate of the centre modes. For flows which satisfy (2.3)–(2.4) we can therefore deduce that a centre-mode neutral curve is given simply by

$$|Q| = 1. \tag{3.16}$$

The quantity Q is obtainable numerically purely from the outer-region problem, for which one sets $\epsilon = 0$, and so Q depends only on k, m and the mean flow profiles U & W. We will find in §4 below that another portion of the neutral curve is given by $\alpha_0 = 0$.

4. The case of $\alpha_0 > 0$ and stable centre modes

In this section we rework the calculation of §3, only now under that assumption that

$$\alpha_0 \equiv \mu^2 > 0, \tag{4.1}$$

again looking for frequencies

$$\omega = \omega_c(0) + \epsilon, \tag{4.2}$$

with $|\epsilon| \ll 1$. We shall find in these cases (with $\alpha_0 > 0$) that $\epsilon \in \mathbb{R}$ and the centre modes are stable. To proceed we could rework the arguments of the previous section one after another. The problem is very similar, however, and we can use this to simplify the presentation of the stable centre-mode asymptotics.

We again have the same asymptotic regions as defined in table 1, and by substituting $v \to i\mu$ the solutions (3.5), (3.8) and (3.11) in the three regions all carry over. The qualitative difference is that now the outer-region solutions have the form

$$g_{\pm}(r) \sim r^{-1/2} \exp\left\{ \pm \frac{2\nu \mathrm{i}}{r} \mp \frac{3r\mathrm{i}}{16\nu} \right\} \quad \text{as} \quad r \to 0, \tag{4.3}$$

and are of the same order of magnitude if $r \in \mathbb{R}$. The matching procedure between the intermediate and outer regions now formally takes place as $r \to 0$ through real values. Since v must be real for $r \in \mathbb{R}$, let us define two alternative outer-region solutions $G_{\pm}(r)$, where

$$G_{\pm}(r) \sim r^{-1/2} \sin(\Theta),\ r^{-1/2} \cos(\Theta) \quad \text{as} \quad r \to 0, \tag{4.4}$$

with $\Theta \equiv 2\nu/r$.

We can now perform the matching: applying the outer-region boundary condition will determine an $O(1)$ and real constant P such that

$$v \propto G_{+}(r) + PG_{-}(r) \quad \text{in the outer region}, \tag{4.5}$$

to be matched with the intermediate-region solution (3.8). We obtain, analogous to (3.14),

$$\epsilon = \frac{-\mu^2 \omega_c''}{2n^2} - \frac{\mu^2 \omega_c''}{2n^3} \left(\frac{1}{\pi} \tan^{-1} \left(\frac{2P}{P^2 - 1} \right) - |m| - \frac{1}{2} \right) + O(n^{-4}). \tag{4.6}$$

Since P must be real (4.6) implies centre modes which are stable to $O(n^{-3})$, and indeed all higher terms in the expansion are also real, and the modes genuinely are stable. This is clear because we never need to depart from real values of r in this section, and the entire problem is consequently real. If we were to fully rework the arguments of § 3 and include all the algebra, then in each asymptotic region we would define real solutions, such as (4.4), in place of the complex solutions, such as (3.5), (3.8), and (3.11). Since we now consider only real r, the coefficients of all the real solutions and the matching results would also be real.

Provided the real frequencies given by (4.6) are permissible, i.e. they do not lie in the continuous spectrum, then an infinite number of stable centre modes lie on the real axis in the ω-plane and accumulate towards $\omega_c(0)$. If $\omega = \omega_c(0)$ is a global extremum of $\omega_c(r)$ over all radii in the flow, then this will be the case. If $\omega_c(0)$ is in the interior of the continuous spectrum, then centre modes are not present when $\alpha_0 > 0$.

Figure 1(*b*) shows the positions of the regular singular points for stable centre modes as given by (4.6). It is seen *a posteriori* that matching and approaching $r = 0$ on the real line is indeed natural. As in § 3 the Frobenius exponents are large and real as $\epsilon \to 0$, giving rise to rapid oscillations in the intermediate region.

5. Centre modes for the Batchelor vortex

We adopt the Batchelor vortex as a test case to demonstrate the theory we have presented for inviscid centre modes. A large number of authors have considered the

stability of this flow in various regimes and a review of some of the most relevant literature is given in § 1 above. The strongest instability modes, across all parameter regimes, have previously been found to be inviscid in character; we shall see how the analysis of § 3 applies to these modes, in agreement with previous numerical results and also asymptotic studies of certain parameter limits. The strong inviscid modes are not, however, universally responsible for vortex breakdown, as they are restricted to relatively small levels of mean swirl. In addition to the discussion of the strong instabilities, which lie in the heart of the unstable region, we shall therefore also explore in detail the location of the neutral curve for inviscid instabilities. Of particular interest is the swirl level above which all inviscid modes are neutralized.

We now apply the results of § 3 and § 4 to the Batchelor vortex. The mean flow is taken to be

$$\left.\begin{array}{rcl} U(r) & = & a + \mathrm{e}^{-r^2}, \\ W(r) & = & q\left(1 - \mathrm{e}^{-r^2}\right)/r, \end{array}\right\} \tag{5.1}$$

defined by swirl parameter q and advection parameter a. We consider temporal stability, and so without loss of generality we may consider $a = 0$ from here on by applying a Galilean transformation.

Substituting (5.1) into (2.16), we obtain the expected form (2.17) with

$$\alpha_0 = \frac{kq(kq+m)}{(k+mq/2)^2}. \tag{5.2}$$

Restricting to the case $m < 0$ and $q > 0$, which has previously been shown to be the most important region for the inviscid instabilities, it follows that $\alpha_0 < 0$ and unstable centre modes may be possible for

$$0 < k < |m|/q. \tag{5.3}$$

Another stability boundary for the centre modes of § 3 is given by (3.16); finding this boundary requires a numerical solution of the leading-order outer-region problem of § 3.3, i.e. solution of (2.9) with $\omega = \omega_c(0) = k + mq$, so that $\epsilon = 0$ in (3.2). We shall return to the question of the neutral curve shortly, after we first give some numerical calculations of spectra to demonstrate that the centre-mode structure of § 3 and § 4 is indeed present.

5.1. *Numerical calculations of spectra*

We numerically integrate (2.9) with standard error-controlling variable-step-size integrators in the MATLAB™ computing environment. After applying the appropriate boundary condition (2.10)–(2.11) at $r_{\min}$ (typically 10^{-3}) we integrate up to $r = r_{\max}$ (typically 20) and check to see if the second boundary condition, $v(r_{\max}) = 0$, is satisfied. Using Newton iterations and an initial guess for the eigenfrequency we converge on a mode in typically 5–10 iterations. The error tolerances in the numerical integration, $r_{\min}$ and $r_{\max}$ are all varied to ensure satisfactory numerical convergence. In some cases it proves convenient to deform the numerical integration contour off the real line into the complex r-plane; we may do this provided the contour is not deformed through a singularity r_c for which (2.8) holds. For instance, recall figure 1(*a*) and that unstable centre modes will have RSPs with large Frobenius exponents close to the real line. For such a case, by deforming the integration contour from the real line onto the dashed line shown in figure 1(*a*), so that no singularities are crossed, we can avoid approaching closer to the RSP than necessary and this significantly aids

numerical calculation. A discussion of the locations of the RSPs for the Batchelor vortex is given in the Appendix. Such contour deformation has been employed by several previous investigators.

Our principal numerical method, as outlined in the preceding paragraph, is of the classical 'shooting' type. In contrast, Mayer & Powell (1992) and most recent authors have favoured a pseudospectral (or spectral collocation) method. We shall find that the differences between the two methods are important for resolving the asymptotic structure described in § 3 and § 4, so we devote some time here to a careful comparison of the two methods. The shooting method can be highly accurate, especially when implemented with an error-controlling variable-step-size integrator and when tailored to the problem by careful contour deformation. However, the primary disadvantage of shooting is that only one eigenfrequency is considered at a time. For each individual case any contour deformation must be checked to be valid, a good initial guess must be supplied to initiate the Newton iterations, and then the calculation can proceed. Consequently, large-scale calculations and exhaustive sweeps of parameter space are relatively slow and cumbersome. A pseudospectral method approximates the eigenvalue problem by a matrix system, and then this system is solved to give all the modes for a given set of parameters in a single step. Since all modes are found at once and no initial guess is required, pseudospectral methods are especially useful for large-scale computations. Accuracy can be improved by including more basis functions and thereby generating larger matrices, and can be targeted at specific locations by stretching the coordinate system to concentrate the collocation points. On the whole, however, very high accuracy on a small portion of the radial domain is achieved more easily and dynamically by a shooting method. Pseudospectral methods also have one drawback, which is particularly relevant here: in attempting to resolve the continuous spectrum by a finite matrix problem a large number of 'spurious eigenvalues' result, densely clustered around the true location of the continuous spectrum, C_ω. The spurious eigenvalues are often easy to identify (for instance by repeating the calculation with 10% more basis functions and comparing results), and hence remove. Removing the spurious results has proved successful and perfectly satisfactory for many problems (Mayer & Powell 1992; Fabre & Jacquin 2004). It is also possible to shift the location of the spurious modes to some extent by performing collocation on a deformed contour of integration. However, if one wishes to investigate the immediate vicinity of the continuous spectrum the shooting method is preferable. Shooting produces no spurious results, and in principle shooting can proceed for all $\omega \notin C_\omega$, and fails only for those $\omega \in C_\omega$. More stringent error tolerances are required to find eigenfrequencies closer to C_ω, but the advantage that a correctly implemented shooting approach does not give spurious modes remains. In what follows we must investigate the immediate vicinity of the continuous spectrum in order to demonstrate asymptotic accumulation of eigenfrequencies as predicted by § 3 and § 4. Also, our study of the neutral curve will require inspection of the vicinity of C_ω, because the instabilities become neutral by approaching, and then disappearing into, C_ω as parameters are varied (in fact, they move onto the other, non-physical, Riemann sheet of the complex ω-plane).

As a check on our shooting routine, a pseudospectral code was used to compare to the shooting results where that was possible, namely for the modes farthest from the continuous spectrum C_ω in figures 2(a), 4(a) and 5(a). Good agreement was obtained away from C_ω, but we found that the immediate vicinity of C_ω could only be investigated by the shooting method, as expected. Our calculations have also been checked by comparing to the results of Mayer & Powell (1992).

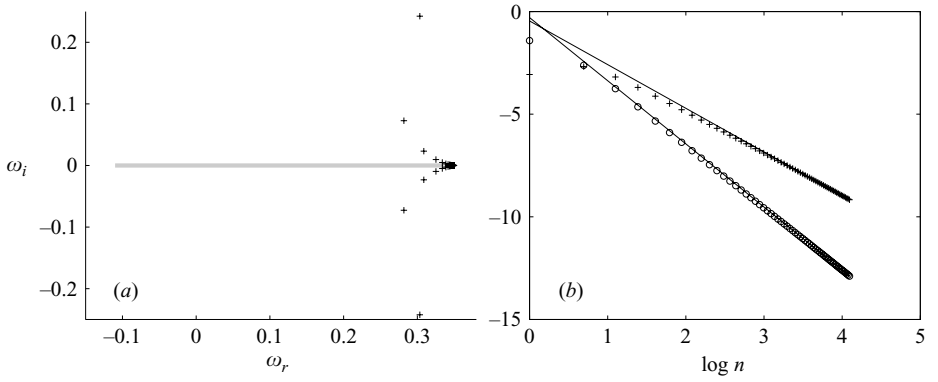

FIGURE 2. (*a*) The frequency spectrum for $(m, q, k) = (-1, 0.46, 0.81)$. Each + shows a mode, and the location of the continuous spectrum C_ω is indicated by a thick grey line. (*b*) +, $\log(|Re(\epsilon)|)$; ○, $\log(|Im(\epsilon)|)$ against $\log n$. The straight lines in (*b*) have gradients of −2 and −3 for comparison.

5.2. *Unstable centre modes*

We begin by looking at the region of parameter space known (Lessen *et al.* 1974; Mayer & Powell 1992) to possess the strong inviscid instabilities. Our aim is to demonstrate that the known instabilities are members of a larger family which is described by the asymptotic framework of § 3. We will then discuss how the centre-mode description of the instabilities, given by § 3, relates to various results in the existing literature. In particular, we will discuss the relation to the $|m| \gg 1$ asymptotics of Leibovich & Stewartson (1983).

We present our first numerical results for the case $(m, q, k) = (-1, 0.46, 0.81)$. These parameters correspond to the strongest inviscid instability for which $m = -1$, having a growth rate of $Im(\omega) = 0.2424$ (see Mayer & Powell 1992, table 2). The strongest mode was satisfactorily recovered by both our shooting and pseudospectral codes. The full results of the shooting calculation are shown in figure 2. The shooting method accurately finds over 60 unstable modes in this case and these are shown in figure 2(*a*), together with their stable complex conjugates. The continuous spectrum C_ω for these parameters is given by $-0.11 \leqslant \omega \leqslant 0.35$, and its location is indicated in figure 2(*a*) by a superimposed thick grey line. Figure 2(*b*) examines the dependence of ϵ on the mode number n, where ϵ is defined by (3.2) and note that $\omega_c(0) = 0.35$ in this case. The mode with largest $|\epsilon|$ is numbered $n = 1$, and subsequent modes are numbered in order of decreasing $|\epsilon|$ (which is equivalent to order of decreasing $|Im(\omega)|$, noting figure 2*a*). Figure 2(*b*) shows that the power laws for $Re(\epsilon)$ and $Im(\epsilon)$ predicted by (3.14) are realized; further, the coefficient of the leading-order n^{-2} term was −0.41 for the numerical results, which compares favourably with the predicted value of $\nu^2\omega_c''/2 = -0.40$ for these parameters. Inspection of the eigenfunctions for the modes shows that they are strongly peaked and increasingly oscillatory close to the axis, in the manner predicted. As an example, figure 3 shows the eigenfunction for the unstable mode $\omega = 0.334 + 0.00482\mathrm{i}$, for which $n = 5$. The predicted radius of localization (3.15) has the value $\nu/n = 0.166$ for the mode in figure 3, which compares well with the numerical eigenfunction. We conclude that the instabilities for these parameters form an infinite family of centre modes as described by the analysis of § 3. Similar numerical investigations of other parameter values have produced similar

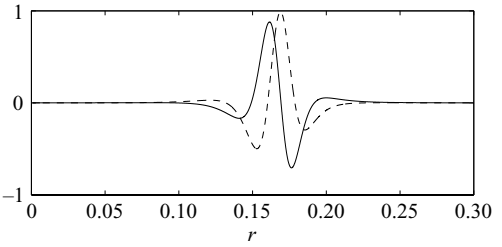

FIGURE 3. The eigenfunction $v(r)$ for the $n=5$ unstable mode of figure 2. Solid line: real part, dashed line: imaginary part.

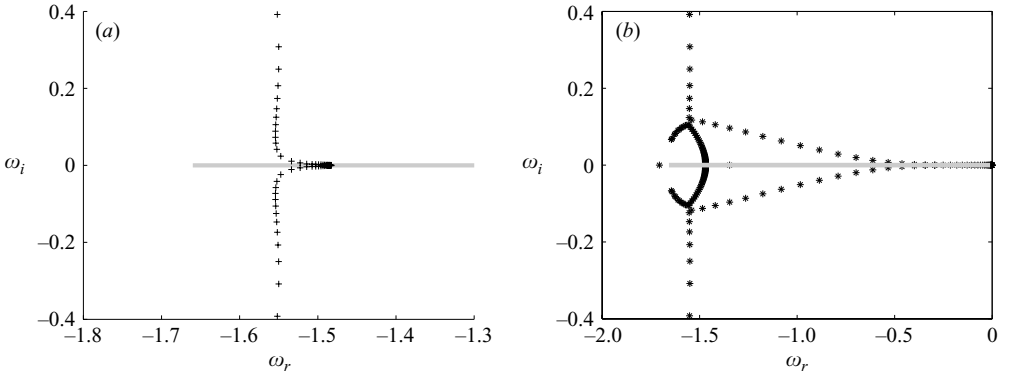

FIGURE 4. The frequency spectrum for $(m, q, k)=(-5, 0.83, 0.2.70)$ found by (*a*) shooting, (*b*) a pseudospectral method with 100 basis functions. In both the location of the continuous spectrum C_ω is indicated by a thick grey line, and each symbol shows a numerically determined mode.

results, and we therefore claim that the asymptotic structure of § 3 applies generally to previously reported inviscid instabilities.

For a further example of the unstable modes we consider $(m, q, k)=(-5, 0.83, 2.70)$, the parameters corresponding to the strongest $m=-5$ instability (Mayer & Powell 1992, table 2). Figure 4(*a*) shows the spectrum, with the primary mode in agreement with Mayer & Powell's result, and the higher-order modes accumulating towards $\omega_c(0)=-1.47$ in the characteristic fashion described by (3.14). It is convenient at this point to digress briefly, and to use this example to clarify the comments made in § 5.1 about the differences between shooting and pseudospectral calculations. Figure 4(*b*) shows the results of a calculation made with 100 spectral basis functions for the same parameter values. We see that the first 6 unstable modes are accurately resolved, and that a cloud of spurious eigenvalues surrounds the vicinity of the continuous spectrum. Figure 4(*b*) is significantly quicker to produce than figure 4(*a*), so if one is interested in just the primary, or even just the first 6 modes, then the pseudospectral method is preferable because the spurious results in figure 4(*b*) can be easily removed by standard methods. However, the spurious modes are actually concealing the finer mathematical structure visible in figure 4(*a*), which is exactly the detail we wish to display. Hence, removing the spurious pseudospectral modes is not sufficient for the present purpose, and so shooting, which generates no spurious modes, is preferred here. Now, the parameters for the calculation in figure 4(*a*) were chosen specifically to make a connection between the description of the modes given by § 3 and the successful

$|m| \gg 1$ asymptotics of Leibovich & Stewartson (1983). Table 2 of Mayer & Powell (1992) shows that $|m| = 5$ is sufficiently large that the most unstable disturbance is fairly well described by the $|m| = \infty$ asymptotics. On the other hand figure 4(*a*) shows that the asymptotic process (3.14), involving the $n \to \infty$ limit, is also present. To connect the two, let us label the general eigenfrequencies by $\omega_{(m,n)}$, where $m, n \in \mathbb{Z}$ are the azimuthal order and mode number, respectively. On fixing the azimuthal order m, then § 3 shows that for each m there is an infinite set of eigenfrequencies and that the limit $n \to \infty$, with m fixed, is described by (3.14). Alternatively, if n is held fixed and we let $m \to \infty$, then the analysis of Leibovich & Stewartson (1983) applies, and the mode is described by Leibovich & Stewartson's asymptotics. The two asymptotic limits, of large m and n, are therefore compatible.

From our numerical investigations of the inviscid instabilities presented in figures 2–4, and also many more similar calculations for which the detailed results are not reproduced, we conclude that the description of § 3 applies generally to previously reported instabilities. We have discussed how the asymptotic limit $n \to \infty$, m fixed, is compatible with the limit $m \to \infty$, n fixed, the latter being the regime studied by Leibovich & Stewartson (1983). The existence of the limit $n \to \infty$, with m fixed, also seems to explain the finding (reported in several numerical investigations of the inviscid instabilities, e.g. Duck & Foster 1980; Mayer & Powell 1992) that there are often multiple unstable modes. The pseudospectral calculation in figure 4(*b*) found 6 instabilities, and as many as 10 have been reported for some parameter values (Mayer & Powell 1992). The explanation is simply that there are infinitely many modes, but that a pseudospectral (or finite difference, in the case of Duck & Foster 1980) matrix method conceals a varying number of the higher modes. The aim of our presented results is, in part, to show that the asymptotics of § 3 and § 4 allow more complete pictures of the spectrum to be drawn: the spectrum comprises a continuous spectrum plus discrete modes of varying types, figures 2(*a*) and 4(*a*) being examples with unstable centre modes.

5.3. *Other modes*

We now take a small diversion from the question of instability (the main physical problem of interest) to discuss the stable centre modes described in § 4. We require $\alpha_0 > 0$ and $\omega_c(0)$ to be a global extremum of $\omega_c(r)$ to obtain stable centre modes as described by § 4. If we consider, as before, $m < 0$ and $q > 0$, then this reduces to

$$\left.\begin{aligned} k > |m|/q \quad &\text{and} \quad k > |m|q, \\ \text{or } k > |m|/q \quad &\text{and} \quad k < |m|q/2. \end{aligned}\right\} \tag{5.4}$$

Figure 5(*a*) shows the spectrum for $(m, q, k) = (-1, 3, 1)$, which demonstrates the asymptotic behaviour (4.6). In this case $\omega_c(0) = -2$, and we find a large number of stable centre modes accumulating as predicted; the first 100 modes are plotted in the figure, after which the shooting calculation was terminated. An example eigenfunction, the $n = 5$ stable mode, is plotted in figure 5(*b*). For larger n the modes are increasingly oscillatory near the vortex axis. Figure 5(*b*) contrasts with figure 3, the corresponding picture for an unstable centre mode, which is strongly localized at a small but non-zero radius. The differences are best explained by recalling figure 1 and the differing locations of the RSPs. Alternatively, note that the argument of the exponential in the intermediate region solution (3.8) is real to leading order for unstable centre modes, but imaginary for stable centre modes; hence the unstable modes grow exponentially in the intermediate region, causing the strong localization. The results presented in figure 5 are typical of our numerical investigations, and we conclude that the

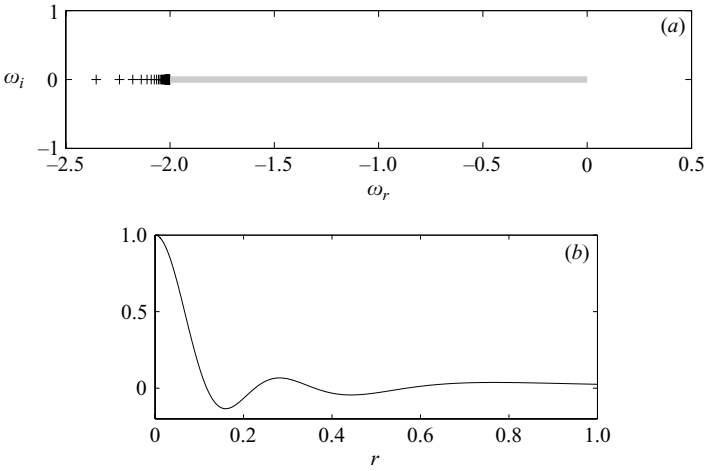

FIGURE 5. (*a*) The frequency spectrum for $(m, q, k) = (-1, 3, 1)$ (*b*) The eigenfunction $v(r)$ for the $n = 5$ stable mode of (*a*).

description of § 4 applies for all suitable parameter values. We note that similar stable centre modes were predicted by Leibovich, Brown & Patel (1986) in the limiting case $0 < kq(kq + m) \ll 1$, a limit which can be realized by long-wavelength modes, for instance. Recalling (5.2), the analysis of § 4 is seen to be compatible with that of Leibovich *et al.* (1986). Indeed, we see that such stable centre modes exist over much of parameter space, and not only for limiting parameter values.

Finally, we mention for completeness that a further type of mode is also possible, namely the ring modes which are described in I. Ring modes are possible when an extremum of $\omega_c(r)$ occurs for a radius in the interior of the flow. Numerically we observed families of ring modes for various parameter values; however, they are not the focus of the present paper. Indeed, for our investigation of the Batchelor vortex neutral curve at small m (and in particular $m = -1$) in the next subsection, they play no part whatsoever. All the unstable ring modes we found for small m were confined to a small region of parameter space within the region of unstable centre modes, and also had much weaker growth rates than the corresponding centre modes. As a specific example, let us discuss $m = -1$, which is the case for which we shall present detailed results in the following subsection. Unstable ring modes are possible for the inviscid Batchelor vortex when $m < 0$ for $q/2 < k/|m| < 1/q$. For $m = -1$ they were observed in the small subset of the unstable parameter space shown in figure 6. In figure 6 the neutral curve calculated by Mayer & Powell (1992) is reproduced to indicate that the ring modes are restricted to a small sub-region of the instability region. In fact, we will show in § 5.4 that the instability region is somewhat larger than the dashed line in figure 6. The unstable ring modes in figure 6 also have much smaller growth rates (of the order 10^{-5}) than the most unstable centre mode at the same parameter values. The ring modes are not amongst the modes found by any of the previous investigators: being so close to the continuous spectrum (because of the small growth rates) the unstable ring modes are only accessible with a shooting method using an appropriately deformed contour.

For clarity and completeness, then, the ring modes and stable centre modes have been mentioned but, as we now focus our attention on the question of the small-m stability boundaries, they will not be discussed any further. To reiterate, unstable ring

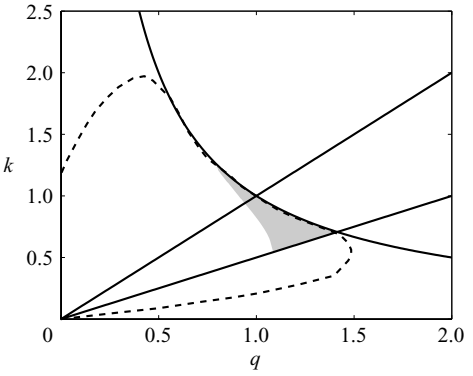

FIGURE 6. The (q, k)-plane for the case $m = -1$. Solid lines show $k = 1/q$, q and $q/2$. The dashed line shows the region of instability found by Mayer & Powell (1992). The grey shading indicates the region containing unstable ring modes.

modes exist in a small subset of the unstable region for centre modes, and where they do exist they have much smaller growth rates than the corresponding unstable centre modes. It is the unstable centre modes which have the largest growth rates and which are present over the entirety of the unstable region.

5.4. *The stability boundary of the inviscid Batchelor vortex*

We now investigate the stability boundary, or neutral curve, of the inviscid Batchelor vortex for small m. Having described the asymptotic theory of unstable centre modes, and a numerical shooting technique which can capture the asymptotic structure, we apply these to the problem of the neutral curve. We investigate in detail the case $m = -1$ in this subsection.

Consider first the boundaries predicted by § 3 for the existence of an infinite family of unstable centre modes. One such boundary is given by $\alpha_0 = 0$, which by (5.2) gives three possibilities: $k = 0$, $q = 0$ and $k = 1/q$. The second such boundary is (3.16), i.e. $|Q| = 1$. The quantity Q relates to the leading-order outer-region problem, so to determine it we set $\epsilon = 0$ in (3.2) and proceed. Now, for $\epsilon = 0$ the two RSPs depicted in figure 1(*a*) are coincident and located at the origin $r = 0$. We integrate (2.9) numerically from an outer boundary $r_{\max}$, where the condition $v(r_{\max}) = 0$ is applied, towards the origin. Formally, using the arguments of § 3, we must follow a contour akin to the dashed line in figure 1(*a*) until $|r| = \delta \ll 1$, and then extract from the numerical data coefficients of the two exponentials (3.11) and hence determine Q via (3.12). Although this procedure was found to work, it is computationally expensive to resolve the very fast oscillations of (3.11) for small and imaginary values of r. Instead, the following more efficient procedure, which is mathematically equivalent, was used.

(*a*) First integrate (2.9) from $r = r_{\max}$ to $r = 1$ along the real axis.

(*b*) Integrate from $r = 1$ to $r = \delta \ll 1$ along the real axis, and extract the coefficient of g_+, the exponentially growing solution.

(*c*) Integrate from $r = 1$ to $r = -1$ along the semi-circular contour $r = \mathrm{e}^{\mathrm{i}\theta}$, $0 \geqslant \theta \geqslant -\pi$.

(*d*) Integrate from $r = -1$ to $r = -\delta$ along the negative real axis, and extract the coefficient of g_-, which is exponentially growing as $r \to 0$ through negative values.

The two coefficients of $g_\pm$ are then combined to calculate Q using (3.12). For our numerical calculations the value of δ was reduced until satisfactory convergence was obtained for the value of Q. Typically $\delta = 0.1$ was found to be sufficient for the

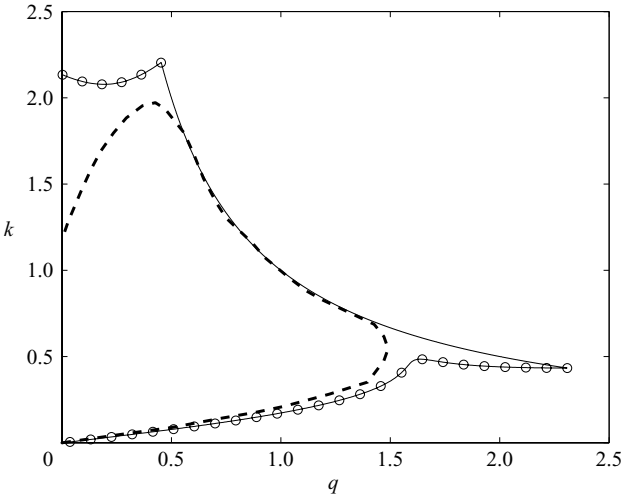

FIGURE 7. The (q, k)-plane for the case $m = -1$. The dashed line shows the neutral curve found by Mayer & Powell (1992). The solid line shows the predictions of § 3: $k = 1/q$ (solid line with no symbols) and $|Q| = 1$ (solid line overlaid with ∘ symbols).

exponentially growing solution to be dominant and to yield an accurate value for the coefficient.

The calculation of $|Q|$ is thus relatively straightforward, and the results are shown in figure 7. The calculated curve $|Q| = 1$ is shown in the figure overlaid with symbols to differentiate it from the other predicted neutral curve $k = 1/q$, and the symbols are merely for clarity of presentation. The curve $|Q| = 1$ was calculated and plotted using many more points than the number of ∘ symbols in the figure.

Before commenting on figure 7 we shall also present the results of a purely numerical determination of the neutral curves of the centre modes, found using our specially tailored shooting method. The strategy here was first to identify an unstable mode at a location comfortably in the interior of the unstable region, where the growth rates are large enough for both shooting and pseudospectral codes to be used and compared. Then we track this mode towards the neutral curve by incrementally changing q and k and at each step performing a new shooting calculation with an initial guess derived from the eigenfrequency at the previous step. A deformed integration contour was again used to aid the computation. We found that the curve $k = 1/q$ accurately described one portion of the neutral curve. Figure 8 shows the numerically determined neutral curves for the primary, secondary and senary unstable centre modes (i.e. those with $n = 1$, 2 and 6, respectively) and how these compare to the $|Q| = 1$ curve. Very close agreement is found, with the single exception of the primary mode in figure 8(a). The general trend is that on approaching the neutral curve the primary mode stabilizes first, followed by the secondary and higher-order modes in order. The neutral curves of the higher modes become closer and closer to the $|Q| = 1$ boundary. By the time the senary mode (i.e. with $n = 6$) is considered, the computed neutral curve is almost indistinguishable from the $|Q| = 1$ curve.

In order to interpret figures 7 and 8 it is timely to reconsider exactly what the condition $|Q| = 1$ means in terms of the asymptotic theory of § 3. It is clear that each mode in the infinite set of centre modes must have its own neutral curve. Rather than exactly describing any one of the modes, (3.14) relates to the $n \to \infty$

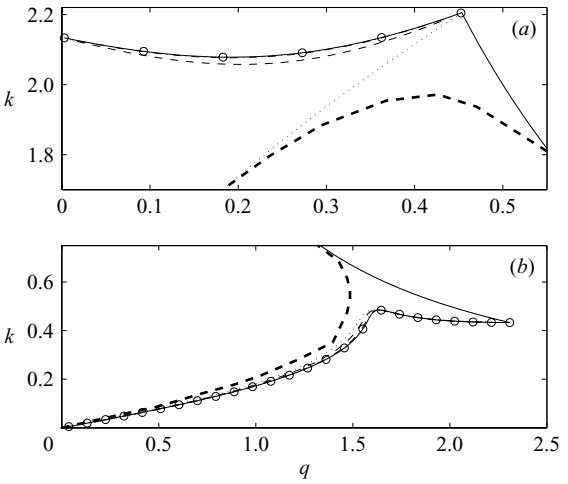

FIGURE 8. Close-ups of the (q, k)-plane for the case $m = -1$. Solid and thick dashed lines as in figure 7. The dotted, dashed and dash-dotted lines show the neutral curves of the primary, secondary and senary centre modes respectively.

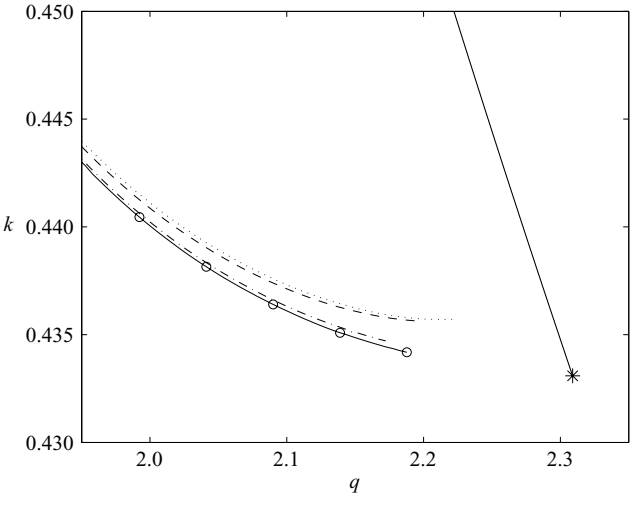

FIGURE 9. Close-up of the (q, k)-plane for the case $m = -1$. All lines have the same meaning as in figure 8. The $*$ symbol shows the upper neutral point as predicted by Stewartson & Brown (1985).

limit. Hence $|Q| = 1$ is to be interpreted as the stabilization of the infinite tail of the high-order modes. Our numerical computations shown in figure 8 find that the low order (primary, secondary etc.) modes stabilize first, followed by the infinite tail. Hence, the neutral curve of the infinite tail of high-order modes, $|Q| = 1$, is in fact the overall neutral curve.

Finally, let us examine the upper neutral point. Stewartson & Brown (1985) performed an asymptotic calculation looking for unstable modes lying on $k = 1/q$, the solid line without symbols in figures 7–9. They predicted that the upper neutral point would lie on this line with $(q, k) = (2.31, 0.433)$. Figure 9 shows a close-up of our results at the upper neutral point. Our numerical methods can track the neutral

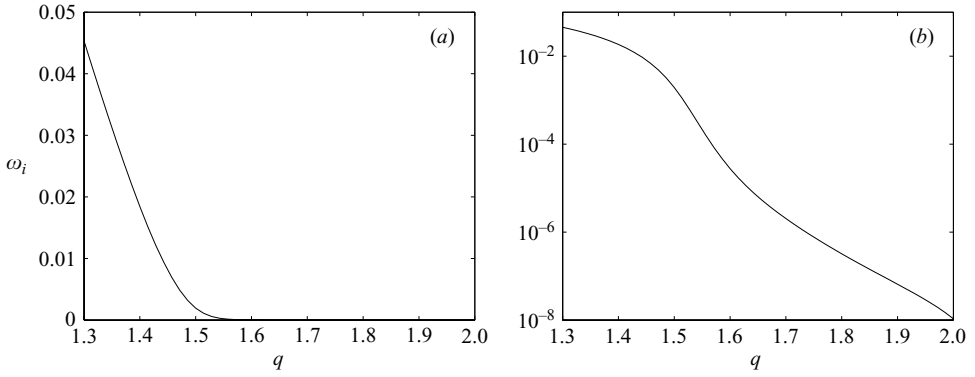

FIGURE 10. (*a*) For $m = -1$, the growth rate of the primary mode along the line segment between $(q, k) = (1.3, 0.6)$ and $(2, 0.45)$ (i.e. $k = (123 - 30q)/140$). (*b*) The same as plot (*a*), shown with a logarithmic scale.

curves very close to neutrality, but are unable to continue beyond what is plotted in the figure as the growth rates become too small. The solid lines showing the two neutral curves derived in § 3 (that is, $|Q| = 1$ and $k = 1/q$) appear on course to intersect at the * symbol, in agreement with Stewartson & Brown's result. Our numerically computed neutral curves in figure 9 show the primary, secondary and senary modes being stabilized at values of q approaching 2.31 from below, which is the first numerical confirmation of $q = 2.31$ as the upper neutral point. Overall, the agreement between our asymptotic and computed neutral curves, and also their agreement with Stewartson & Brown's result at the upper neutral point, leads us to conclude that the neutral curve is correctly given by the solid lines in figure 7. In particular, the upper neutral point is indeed at $q = 2.31$, in agreement with Stewartson & Brown's principal result. Stewartson & Brown's more detailed results further predicted that for $q < 2.31$ neutral modes exist on the line $k = 1/q$ only in discrete intervals of q, implying small deviations of the neutral curve from $k = 1/q$. It was not numerically possible to confirm this detail, however, and their asymptotic analysis remains the best guide to this.

The results presented have concentrated on the case $m = -1$, in order to give as full an account as possible of the (q, k)-plane, and also to allow us to discuss the upper neutral point (the overall upper neutral point, over all m, occurs for $m = -1$). The inviscid Batchelor vortex is similarly unstable for all $m < 0$ and analogous detailed calculations to those presented for $m = -1$ were also performed for $m = -2, -3$. Similar results were obtained, with the unstable region larger than previously reported and the maximum q for inviscid instability in agreement with Stewartson & Brown's predictions of $q = 2.11, 1.99$ respectively.

Finally, let us return to the $m = -1$ case. The neutral curve we have found differs from that of previous numerical investigations, so let us inspect the newly found instabilities. The upper neutral point has been a question of particular interest, and it is at this point that the solid and dashed lines in figure 7 differ most. Figure 10 shows the growth rate of the primary ($n = 1$) unstable mode along the straight line segment from $(1.3, 0.6)$ to $(2, 0.45)$ in the (q, k)-plane, which starts within Mayer & Powell's neutral curve; see figure 8(*b*). The growth rate is seen to drop dramatically for $q \gtrsim 1.5$, though it remains positive because the line segment lies entirely within the unstable region. The dramatic drop in growth rate can largely be explained by the peculiar shape of the instability region, which extends to larger q only in a very

narrow tongue. Modes lying in this tongue are simultaneously close to two different branches of the neutral curve, and so growth rates are much smaller than would be found a similar distance from other segments of the neutral curve. If distance from the neutral curve is considered as a small parameter, say $\beta \ll 1$, then growth rates in the narrow tongue will be $O(\beta^2)$, compared to the more typical $O(\beta)$ at the rest of the neutral curve. For example, there is no such dramatic reduction in $Im(\omega)$ near the upper portion of the $|Q| = 1$ neutral curve in figure 7. In the context of investigating the mathematical structure of the inviscid problem, the peculiar shape of the neutral curve, and the very small growth rates at larger q, explain why determining the neutral curve has proved a difficult problem. In the wider context of vortex stability and breakdown, the weakness of the instabilities at larger q will restrict the direct relevance of those modes, something we discuss below.

6. Conclusions

We have presented a theory of inviscid modes with a centre-mode structure, and applied it to the much-studied case of the Batchelor vortex. Inviscid modes are of course only one aspect of vortex breakdown, but within the context of the inviscid problem the asymptotic theory presented gives some new understanding. Much study has been directed at problems of vortex stability. It is hoped that the combined results of I and the current paper give a thorough mathematical account of the inviscid problem, and that this will complement the work in other (e.g. viscous) regimes.

Thinking specifically of the Batchelor vortex case study, we have found that the inviscid instabilities previously found numerically, and studied asymptotically in many parameter limits, are generally centre modes of the type described. The instabilities can be classified as centre modes throughout the unstable region, and the inviscid spectrum typically looks like figure 2(a). In different respects this analytical framework agrees with the results of others, obtained in large-$|m|$, near-neutral (i.e. $kq(kq + m) \simeq 0$), or other parameter limits. As for concrete results, we have presented detailed results for the $m = -1$ neutral curve, and verified numerically that it is given correctly by the centre-mode analysis. The advantages and limitations of both pseudospectral and shooting numerical methods were found to be important in the calculation of the neutral curve, and it seems that care is needed for this problem.

One point of particular note is that our results agree with Stewartson & Brown's (1985) result that the upper neutral point occurs at $q = 2.31$. Numerical calculations have not recovered this result before, which may perhaps be attributed to the peculiar shape of the neutral curve at larger q, and the resulting very small growth rates. The very small growth rates of the newly found instabilities means that they are unlikely to directly affect the bigger picture of vortex breakdown. Figure 4(a) of Fabre & Jacquin (2004) shows that for $m = -1$ and $q = 2$ the primary viscous mode is much stronger than the $q = 2$ inviscid mode of figure 10, for all realistic Re. Also, Fabre & Jacquin found that viscous instability modes occur at any q for sufficiently large values of Re, so there is no 'upper neutral point' for the full viscous problem. Nevertheless it is still important that the precise structure of the inviscid problem is identified, and in the present paper we have determined in detail the location of the inviscid neutral curve. Several numerical and analytical studies of the inviscid problem are now brought together, in particular the most unsatisfactory discrepancy, surrounding the location of the upper neutral point, is resolved. The upper neutral point and the other corrections to the neutral curve have revealed no significant new instabilities. This allows us to conclude, as anticipated, that instability and breakdown observed

at values of $q \gtrsim 2$ is not a direct result of inviscid instabilities, and instead other possible explanations must be explored, such as viscous modes.

Finally, the details of the inviscid problem for swirling flow may be relevant to other future developments.

(*a*) It should be possible to match the mathematical structure of inviscid solutions onto large-Re theory, to complement and compare to recent studies of the viscous modes (Le Dizès & Fabre 2006). For example, consider a small viscous correction, $Re^{-1} \ll 1$, to the structure described in § 3. The continuous spectrum C_ω of the inviscid problem is formally absent and is replaced by a large number of closely packed stable discrete modes. The width of the critical layer scales as $O(Re^{-1/3})$, to be compared with $O(|\epsilon|)$ as the smallest length scale of the centre modes. The theory of § 3 corresponds to $Re^{-1/3} \lesssim |\epsilon|$, and so in view of (3.14) we expect the number N of unstable centre modes to scale as $N = O(Re^{1/6})$.

(*b*) While an infinite tail of instability modes with very small growth rates may be less important than a strong primary mode in the long-time limit, transient growth is a different matter. It is not always clear why transient growth is large in some circumstances and not in others, but preliminary results of our further work suggest that the infinite tail of centre modes (§ 3 and § 4), and also the continuous spectrum (discussed by I), play a major role in controlling the level of transient growth in a vortex breakdown situation. We believe that the mathematical details of the inviscid problem will prove important for this, and work is ongoing.

The author would like to thank Prof. N. Peake for many useful discussions and also Trinity College, Cambridge, for its financial support.

Appendix

In this appendix we discuss the critical radii r_c of the Batchelor vortex, as defined by (2.8) and (5.1). Setting $u = r_c^2$, (2.8) becomes

$$-\omega + k(a + \mathrm{e}^{-u}) + mq(1 - \mathrm{e}^{-u})/u = 0, \tag{A 1}$$

a transcendental equation which must be solved numerically in general. Solving (A 1), and thus finding the RSPs, was required to ensure that no integration contour was deformed through a singularity in our numerical computations. For our calculations (A 1) was solved using Newton iterations, with a variety of complex initial guesses to ensure that all solutions were found.

Olendraru *et al.* (1999), who also consider the inviscid Batchelor vortex, argue that (A 1) has at most two distinct roots; however, this is incorrect. Specifically, their equation (A7) is a sufficient but not (as is argued) a necessary condition on the solution u. In fact (A 1) admits an infinite number of solutions: the presence of the exponential on the left-hand side of (A 1) means that inverting the equation introduces a logarithmic branch cut. To proceed, let

$$u = b_1 n + b_0 + b_{-1} n^{-1} + \cdots, \qquad |n| \gg 1, \tag{A 2}$$

and substitute into (A 1). Comparing terms of the same order, we find

$$\left.\begin{aligned} b_1 &= 2\pi\mathrm{i}, \\ b_0 &= -\log(\omega/k - a), \\ b_{-1} &= \frac{mq((a+1)k - \omega)}{kb_1(\omega - ak)}. \end{aligned}\right\} \tag{A 3}$$

By taking $|n|$ large, for n both positive and negative, and taking both branches of the square root, we therefore find $r_c \sim \sqrt{2\pi|n|}\mathrm{e}^{\mathrm{i}\theta}$ for $\theta = \pm\pi/4, \pm 3\pi/4$. This can be verified by direct numerical solution of (A 1), using a number of initial guesses for the Newton iterations distributed over a region of the complex u-plane.

REFERENCES

Ash, R. L. & Khorrami, M. R. 1995 Vortex stability. In *Fluid Vortices* (ed. S. I. Green), chap. 8, pp. 317–372. Kluwer.

Batchelor, G. K. 1964 Axial flow in trailing line vortices. *J. Fluid Mech.* **20**, 645–658.

Batchelor, G. K. & Gill, A. E. 1962 Analysis of the stability of axisymmetric jets. *J. Fluid Mech.* **14**, 529–551.

Bender, C. M. & Orszag, S. A. 1978 *Advanced Mathematical Methods for Scientists and Engineers*. McGraw-Hill.

Bers, A. 1983 Space-time evolution of plasma instabilities: Absolute and convective. In *Handbook of Plasma Physics, Vol. 1* (ed. M. N. Rosenbluth & R. Z. Sagdeev), pp. 451–517. North-Holland.

Briggs, R. J. 1964 *Electron-stream Interactions with Plasma*. MIT Press.

Carton, X. & McWilliams, J. 1989 Barotropic and baroclinic instabilities of axisymmetric vortices in a quasi-geostrophic model. In *Mesoscale/Synoptic Coherent Structures in Geophysical Turbulence* (ed. J. Nihoul & B. Jamart), pp. 225–244. Elsevier.

Cotrell, D. L. & Pearlstein, A. J. 2004 The connection between centrifugal instability and Tollmien–Schlichting-like instability for spiral Poiseuille flow. *J. Fluid Mech.* **509**, 331–351.

Delbende, I., Chomaz, J. M. & Huerre, P. 1998 Absolute/convective instabilities in the Batchelor vortex: A numerical study of the linear impulse response. *J. Fluid Mech.* **355**, 229–254.

Denier, J. P. & Stott, J. A. K. 2005 The dominant wave mode within a trailing line vortex. *Phys Fluids* **17**, Art. No. 014101.

Duck, P. W. & Foster, M. R. 1980 The inviscid stability of a trailing line vortex. *Z. Angew. Math. Phys.* **31**, 524–532.

Fabre, D. & Jacquin, L. 2004 Viscous instabilities in trailing vortices at large swirl number. *J. Fluid Mech.* **500**, 239–262.

Heaton, C. J. & Peake, N. 2006 Algebraic and exponential instability of inviscid swirling flow. *J. Fluid Mech.* **565**, 279–318 (referred to herein as I).

Howard, L. N. & Gupta, A. S. 1962 On the hydrodynamic and hydromagnetic stability of swirling flows. *J. Fluid Mech.* **14**, 463–476.

Khorrami, M. R. 1991 On the viscous modes of instability of a trailing line vortex. *J. Fluid Mech.* **225**, 197–212.

Landahl, M. T. 1980 A note on an algebraic instability of inviscid parallel shear flows. *J. Fluid Mech.* **98**, 243–251.

Le Dizès, S. & Fabre, D. 2006 Large-Reynolds-number asymptotic analysis of viscous centre modes in vortices. *J. Fluid Mech.* (submitted).

Leibovich, S. 1978 The structure of vortex breakdown. *Annu. Rev. Fluid Mech.* **10**, 221–246.

Leibovich, S., Brown, S. N. & Patel, Y. 1986 Bending waves on inviscid columnar vortices. *J. Fluid Mech.* **173**, 595–624.

Leibovich, S. & Stewartson, K. 1983 A sufficient condition for the instability of columnar vortices. *J. Fluid Mech.* **126**, 335–356.

Lessen, M. & Paillet, F. 1974 The stability of a trailing line vortex. Part 2. Viscous theory. *J. Fluid Mech.* **65**, 769–779.

Lessen, M., Singh, P. J. & Paillet, F. 1974 The stability of a trailing line vortex. Part 1. Inviscid theory. *J. Fluid Mech.* **63**, 753–763.

Loiseleux, T., Chomaz, J. M. & Huerre, P. 1998 The effect of swirl on jets and wakes: Linear instability of the Rankine vortex with axial flow. *Phys Fluids* **10**, 1120–1134.

Maslowe, S. A. 1974 Instability of rigidly rotating flows to non-axisymmetric disturbances. *J. Fluid Mech.* **64**, 307–317.

Maslowe, S. A. & Stewartson, K. 1974 On the linear inviscid stability of rotating Poiseuille flow. *Phys Fluids* **25**, 1517–1523.

Mayer, E. W. & Powell, K. G. 1992 Viscous and inviscid instabilities of a trailing vortex. *J. Fluid Mech.* **245**, 91–114.

Olendraru, C. & Sellier, A. 2002 Viscous effects in the absolute-convective instability of the Batchelor vortex. *J. Fluid Mech.* **459**, 371–396.

Olendraru, C., Sellier, A., Rossi, M. & Huerre, P. 1999 Inviscid instability of the Batchelor vortex: Absolute-convective transition and spatial branches. *Phys Fluids* **11**, 1805–1820.

Rayleigh, J. W. S. 1916 On the dynamics of revolving fluids. *Proc. Roy. Soc. Lond.* A **93**, 148–154.

Stewartson, K. & Brown, S. N. 1985 Near-neutral centre-modes as inviscid perturbations to a trailing line vortex. *J. Fluid Mech.* **156**, 387–399.

Wang, S. & Rusak, Z. 1996 On the stability of an axisymmetric rotating flow in a pipe. *Phys Fluids* **8**, 1007–1016.